Hexagonal Boron Nitride

International Edition: DOI: 10.1002/anie.201601238
German Edition: DOI: 10.1002/ange.201601238

White Graphene undergoes Peroxidase Degradation

*Rajendra Kurapati, Claudia Backes, Cécilia Ménard-Moyon, Jonathan N. Coleman, and Alberto Bianco**

Abstract: *Hexagonal boron nitride (hBN) nanosheets are emerging as promising 2D materials for different types of applications. However, biodegradation of hBN materials is poorly explored owing to their high chemical inertness and strong oxidation resistance. The assessment of oxidation/biodegradation of hBN is important in developing biomedical tools. Herein, we report the first study on the biodegradability of hBN nanosheets comparing the enzymatic catalysis of two different peroxidases, horseradish peroxidase (HRP) and human myeloperoxidase (MPO), with the photo-Fenton (P.F.) reaction. The results show that degradation of hBN nanosheets is different to that of graphene and graphene oxide, since partial oxidation was found using MPO after 35 h, while HRP failed to degrade hBN up to 60 days. Nearly complete oxidation/degradation was occurred by P.F. reaction in 100 h. These results are helpful in designing advanced conjugates for biomedical uses of hBN.*

The hBN nanosheets, also known as white graphene, belong to the wide family of 2D materials.[1] In addition to hBN and graphene, this family comprises other materials including 2D layered transition-metal dichalcogenides, transition-metal dioxides, and the recently discovered ultra-thin black phosphorous sheets.[2] These types of rapidly emerging materials are promising for various applications in electronics, optics, energy storage, sensors, and catalysis.[1b,2a,3] In addition, they show a great potential in the biomedical field. Since they can be exfoliated and stably dispersed in aqueous media,[1c] such materials can be easily integrated in living systems. Literature evidence suggests that 2D materials will be the next generation of biomedical tools, with performances that seem to surpass those of carbon-based nanomaterials.[4]

hBN is currently extensively explored as an alternative to graphene or in combination with graphene and other 2D materials.[4,5] In the field of biomedical applications, hBN nanosheets are mainly developed for bioimaging and drug delivery systems for anticancer therapy.[6] This use is because highly stable water dispersions, displaying low cytotoxicity, can be obtained using biocompatible surfactants or performing suitable chemical functionalizations on the boron nitride surface.[6] For example, in cancer therapy, hBN was complexed with doxorubicin, showing enhanced cellular toxicity in comparison to the drug alone. In combination with silver nanoparticles, hBN can display antibacterial activity against gram-positive *S. aureus* and gram-negative *E. coli*,[7] although the real effect is mainly due to the presence of silver, rather than to a contribution of boron nitride. One key aspect related to the exploitation of 2D materials in biomedicine is the assessment of their biocompatibility and biodegradability.[8] Indeed, it is of fundamental importance to understand the fate of these materials once administered in vivo. Very little data is available on the cytotoxic effect, although the first reports showed low cytotoxicity.[6] On the other hand, no studies have confirmed the biodegradability of hBN. In the literature, it has been demonstrated that carbon-based materials, such as carbon nanotubes (CNTs), carbon nanohorns, and graphene oxide (GO), are sensitive to the treatment with different types of peroxidases, comprising human peroxidases.[9] Since boron nitride-based materials possess a higher oxidation resistance than graphene,[10] it could be more difficult to degrade BN by peroxidase enzymes unlike carbon derivatives. Based on the lessons learnt from the biodegradation of CNTs[9a,11] and GO,[9b,c] it will be interesting to apply such strategies to degrade hBN in view of its possible biopersistence level in living organisms and the environment. In this context, we have started to elucidate the capacity of different oxidative enzymes to degrade hBN. We have decided to compare three different conditions in which hBN dispersed by sodium cholate might be or might not be degraded. In particular, we have treated hBN with horseradish peroxidase, myeloperoxidase, and UV-assisted photo-Fenton reaction. All three treatments have shown different hBN oxidation profiles arising from the type of reactive intermediates or radicals generated.

hBN nanosheets were produced from bulk BN material by liquid-phase exfoliation.[12] This involves sonication in water using sodium cholate as surfactant similar to our earlier methods[13] (see Supporting Information). hBN/Na cholate suspensions exhibited an excellent aqueous colloidal stability (see left inset in Figure 1). This was also confirmed by its high negative zeta potential (−33.5 mV at pH 7). Atomic force microscopy (AFM) and transmission electron microscopy (TEM) analysis evidenced the production of nanosheets with lateral sizes of 200–600 nm and thicknesses of 1–10 layers (Figure S1,S2 in the Supporting Information).

To interrogate the biodegradability of hBN sheets, we chose three different routes. We first treated hBN dispersion with the plant enzyme HRP,[14] which is a model peroxidase enzyme that generates highly oxidative intermediates. Secondly, we used human myeloperoxidase extracted from human neutrophils, which is a much stronger peroxidase

[*] Dr. R. Kurapati, Dr. C. Ménard-Moyon, Dr. A. Bianco
CNRS, Institut de Biologie Moléculaire et Cellulaire, Laboratoire d'Immunopathologie et Chimie Thérapeutique
15 Rue René Descartes, 67084 Strasbourg (France)
E-mail: a.bianco@ibmc-cnrs.unistra.fr
Dr. C. Backes, Prof. J. N. Coleman
School of Physics and CRANN, Trinity College Dublin
Dublin 2 (Ireland)

Supporting information for this article can be found under: http://dx.doi.org/10.1002/anie.201601238.

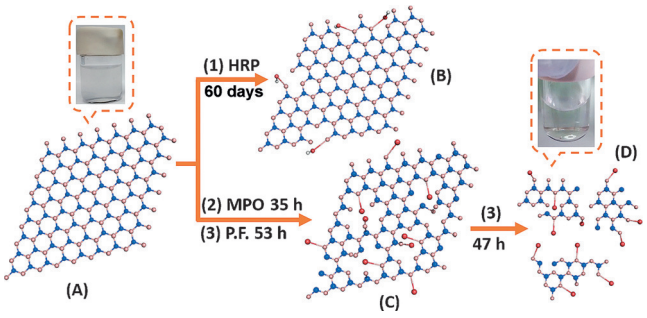

Figure 1. Schematic representation of oxidation/degradation of hBN nanosheets using HRP (1), MPO (2), and P.F. reaction (3), showing possible structures of the resulting BN degradation fragments (B–D). A) Starting hBN nanosheets, B) hBN nanosheets after treating with HRP for 60 days, C) hBN nanosheets after treating with MPO for 35 h (2) or photo-Fenton (P.F.) reaction for 53 h (3), and D) hBN fragments after 100 h of P.F. reaction. The digital photos shown above (A) and (D) show the hBN suspensions at time 0 and after 100 h (end of the process) of P.F. reaction. B gray, N blue, O red.

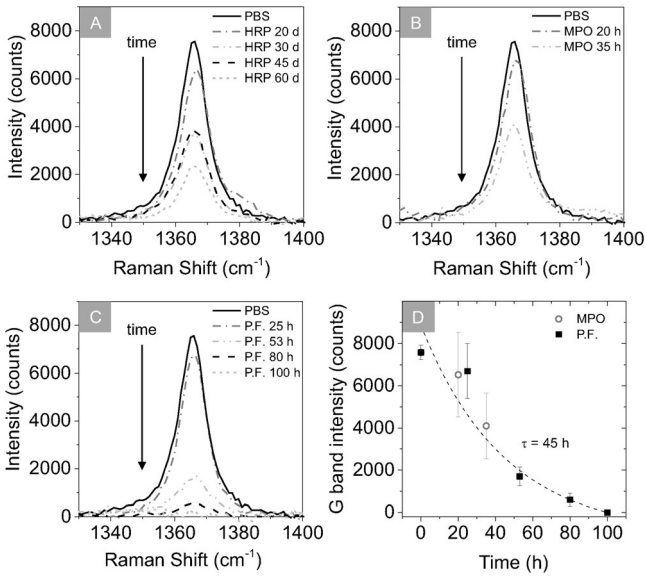

Figure 2. A) Raman spectra of hBN nanosheets treated with HRP, B) treated with MPO, and C) treated by P.F. reaction. D) Plot of the BN G-band intensity as a function of time for MPO- and P.F.-treated samples. The intensity decays exponentially, consistent with degradation.

than HRP able to produce HOCl in addition to its reactive intermediates.[9a] Finally we performed the UV-assisted photo-Fenton reaction that generates the most powerful hydroxyl radicals catalyzed by $FeCl_3$. This method was applied earlier to decompose large aromatic compounds as well as CNTs and GO.[15]

Initially, BN/Na cholate nanosheets (78 μg mL^{-1}) were incubated with HRP in phosphate buffered saline (PBS) and H_2O_2 was added to the suspension one time per day up to 60 days. The color of the hBN suspension (Figure 1, left inset) did not change even at the end of the period (indicating an ongoing degradation process) in contrast to carbon nanomaterial degradation in which case transparent solutions were obtained after 20 days.[9c,14] Next, hBN nanosheets (100 μg mL^{-1}) were treated with human MPO in the presence of NaCl and H_2O_2. In this case, hydrogen peroxide was added every hour for 35 h. Then, the color of the suspension became slightly translucent unlike CNT or GO dispersions, where the typical brownish color disappears within 24 h.[9a,b] Then, P.F. reaction of hBN nanosheets was carried out in the presence of $FeCl_3$ and H_2O_2 at pH 4 under UV irradiation at 365 nm for 100 h.[15a] The hBN suspension changed to a nearly transparent solution (Figure 1, right inset, see also Figure S3) after 100 h. The course of the different degradation processes was followed using complementary spectroscopic (i.e. Raman) and microscopic techniques, such as TEM and high-resolution TEM (HRTEM), as well as X-ray photoelectron spectroscopy (XPS).

Raman analyses were initially carried out to gain detailed information on the oxidation or degradation levels of hBN (see Supporting Information methods and Figure S4,S5) as a function of time. The chemical structure of hBN monolayers is different from other 2D materials, such as graphene. Only the G-band relative to the E_{2g} phonon (B–N vibrational mode) is allowed.[5d,16] This band is located around 1366 cm^{-1}. The oxidation/degradation state of BN nanosheets before and after treatment with HRP, MPO, and P.F. reaction was assessed based on the changes in intensity of the G-band (Figure 2). In the case of HRP treatment (Figure 2A), the intensity of the G-band gradually decreased as treatment increased from 0 to 60 days. In the case of MPO, the G-band intensity also gradually decreased compared to untreated hBN (Figure 2B) within only 35 h. These results suggest that the degradation of hBN is more effective using the MPO/H_2O_2/NaCl system than HRP/H_2O_2 conditions, in agreement with previous studies on CNTs and GO.[11a,17] Indeed, it is established that reactive intermediates of MPO and HOCl are much stronger oxidants than the oxidative species generated by HRP.[9a] Similarly, the P.F. reaction strongly affected the G-band resulting in a gradual decrease in intensity with increasing reaction time from 0 to 100 h (Figure 2C), up to a complete disappearance at the end of the experiment. In particular, the complete absence of the G-band after 100 h treatment supports the full oxidation or degradation of hBN nanosheets. This is likely to be due to the production of strong hydroxyl radical species during the P.F. reaction.[15a] We can analyze the intensity of the G-band as a function of time in all cases (Figure 2D and Figure S5). Despite the scatter in the data as a result of sample inhomogeneity (see Supporting Information methods), it is clear that the G-band follows an exponential decay which is consistent with degradation. Fitting allows time constants for the degradation to be estimated. As already suggested above, the degradation is significantly slower in the case of HRP treatment with time constant on the order of 50 days (Figure S5) compared to MPO and P.F. In the MPO and P.F. cases, the G-band intensity as a function of time falls on the same curve (Figure 2D). Fitting the data to an exponential decay gives a time constant on the order of 45 h.

We also observed an increase in the width of the G-band on degradation. While the G-band can be fitted reasonably

well with single Lorentzians in all cases (Figure S4), it is consistently broadened in the HRP, MPO, and P.F.-treated samples. The full width at half maximum (FWHM) increases from around 9 cm^{-1} in the reference sample up to approximately 11.5 cm^{-1} in the case of the P.F. reaction (Figure S5) further suggesting a disruption in the chemical structure.

The decreasing (reduction in the intensity) as well as broadening of G bands were previously observed for hydroxyl-functionalized hBN sheets via oxygen radical action,[18] and for thermally oxidized BN sheets[5d] including BN quantum dots obtained by oxidation of BN sheets.[16] Although it is still not theoretically clear why the G-band was decreasing during the oxidation of hBN, its reduction in intensity and its broadening can be attributed to an oxidation process,[5d] as the oxidation of BN sheets can reduce the number of the B–N bonds by insertion of oxygen atoms.[5d]

In the next step, we employed TEM to obtain more insights into the degradation of hBN nanosheets using the different oxidative conditions described above (Figure 3). There was no change in the morphology of hBN after treating with HRP/H_2O_2 for 15 days (Figure 3A) in agreement with

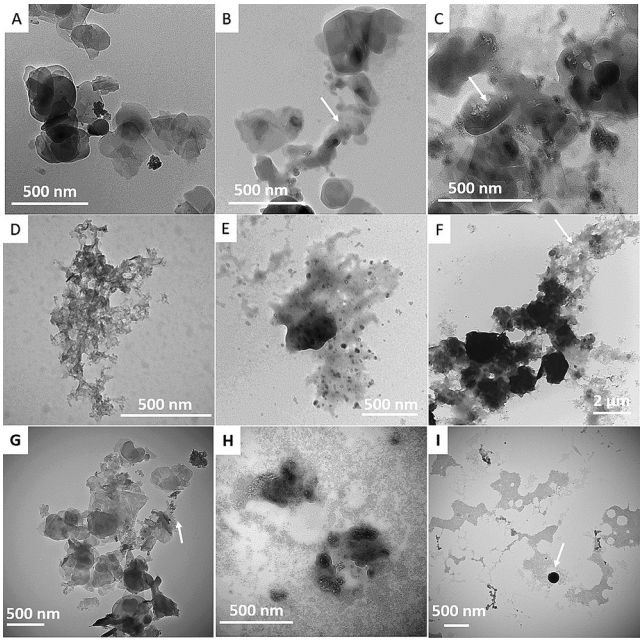

Figure 3. TEM images of BN sheets. The first row shows HRP-treated hBN for 15 days (A), 30 days (B), and 60 days (C). The second row shows MPO-treated hBN for 20 h (D) and for 35 h (E,F). The third row shows hBN after P.F. reaction for 25 h (G), 53 h (H), and 100 h (I). The arrows in (B), (C), (F), and (G) indicate nanopores on the surface of hBN sheets, while the arrow in (I) shows the round shaped particles left after 100 h treatment.

the Raman analysis. However, few tiny pores on the nanosheets were formed after 30 days as indicated by the arrow in Figure 3B. After 60 days, the number of the little pores increased in dimension (Figure 3C). We could notice that the sharp edges of hBN nanosheets became dull in comparison to untreated hBN, likely because the oxidation of BN first occurs at the edges. Compared to GO and CNTs, hBN sheets seem more resistant to the oxidative HRP/H_2O_2 system, since the GO and CNTs were degraded after 20 days,[9c,11a] whereas hBN is still persistent after 60 days. The hBN control sample treated with only H_2O_2 for the same period did not show any changes in the morphology (Figure S6).

Then we analyzed the sample treated with MPO/H_2O_2/NaCl. After 20 h, the flat nanosheets started to become porous (Figure 3D), and their edges were highly crumpled. A further evolution in the morphology occurred in the following 15 h, with drastic changes in the sheets that appeared extremely porous (Figure 3E). In addition, we observed a certain number of nanoscale fragments along with the porous BN sheets, attributed to the cleavage of hBN sheets into nanodot-like structures during the degradation process (Figure 3E). Nevertheless, MPO degradation of hBN was not complete even after 35 h, because many aggregates were still present (Figure 3F). This is in contrast to the behavior of CNTs and GO that could be completely degraded within 24 h by treatment with MPO/H_2O_2/NaCl.[9a] We note that the addition of only H_2O_2 (every hour) did not affect the structure of the nanosheets (Figure S7). These results also emphasize the stronger oxidation resistance of hBN in comparison to materials made of graphite.

HRTEM along with selected-area electron diffraction (SAED) analyses were used to interrogate the changes in the crystallinity and the fine structure of hBN nanosheets after treating with HRP and MPO (Figure S8). Most of hBN layers retained their flat morphology with considerable damage at their edges. The hexagonal single crystallinity of hBN was also preserved even after 60 day HRP treatment as revealed by SAED pattern (Figure S8A, inset).[5a] In addition, few highly porous fragments and amorphous structures were found again supported by the diffuse diffraction SAED pattern (Figure S8B, inset). However, in the case of hBN treated with MPO for 35 h, highly porous sheets were visible (Figure S8C), together with some sheets that completely lost their layered morphology as marked by the arrow. SAED analyses of small porous BN fragments showed a nearly diffused ring pattern with few less intense spots which indicates almost like amorphous structure (Figure S8D, inset). Overall, HRTEM/SAED analyses confirmed that MPO is more potent than HRP to degrade hBN in agreement with the Raman and TEM data. Most probably, the synergistic effect of hypochlorite and the reactive oxidative intermediates of MPO are able to degrade hBN layers more efficiently than HRP/H_2O_2 as reported earlier for CNTs and GO.[9a,b]

Finally, the P.F. reaction was found to affect the structure of hBN more significantly than HRP or MPO as shown in Figure 3G to 3I. No evident morphological changes were observed after 25 h (Figure 3G), except formation of few pores at the edges of some BN sheets. However, after 53 h a large number of holes appeared on the surface of BN surface (Figure 3H) leading to the loss of the typical flat morphology. Finally, by 100 h reaction, the majority of BN sheets were converted into highly porous fragments, where the 2D sheet layered motif of hBN was completely lost (Figure 3I). In addition to these fragments, few round shaped and thick particles including some partially degraded and aggregated sheets were also present (Figure 3I and Fig-

ure S9). No such degradation was observed in the reference experiments (Figure S10). The effective degradation of hBN by the P.F. reaction is in good correlation with the Raman analysis (Figure 2C). The stronger oxidation resistance of hBN compared to graphene was also confirmed in the case of the P.F. reaction, since BN sheets were nearly fully degraded after 100 h, while GO required half this time to complete the same process in similar conditions.[15d] Overall, by comparing the three degradation methods, the P.F. reaction was found to be the most effective, followed by human myeloperoxidase.

To further confirm the efficient degradation process by the P.F. reaction, the remaining products of the hBN oxidation process (obtained by precipitation of the samples by adding NaCl, see Supporting Information) were analyzed by X-ray photoelectron spectroscopy (XPS; Figure 4). The results clearly emphasize the strong oxidation of BN sheets, since the atomic percentages of B and N were significantly decreased after 40 h of treatment, with a simultaneous exponential increase of the percentage of oxygen (Table S1 in Supporting Information).

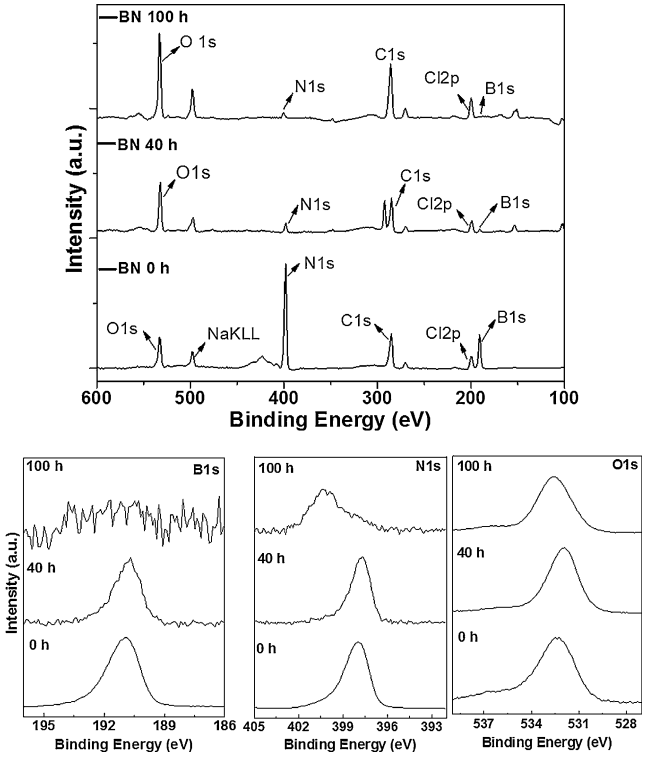

Figure 4. XPS spectra of hBN sheets. Top: Survey spectra of hBN nanosheets at 0, 40 and 100 h of P.F. reaction. Bottom: Core-level spectra of B1s, N1s, and O1s of hBN at 0, 40, and 100 h, respectively.

At 0 h, the atomic percentages of B, N, and O were 46.5, 42.9, and 10.6%, respectively. After 40 h, these percentages changed to 18.8, 17.1 and 64.1%, respectively. At the end of the experiment, the value for B and N decreased to 3.9 and 9.0%, while that of O was 87.1%. The signal intensities of the core-level spectra of B1s and N1s were drastically decreased (Figure S11) and their peak shapes were deformed as the reaction time increased from 0 to 100 h. Particularly, the shape of B1s peak disappeared at the end of the experiment, while the shape of N1s was shifted to higher energy compared to 0 h, which could be due to the presence of N–H bonds as reported elsewhere during the oxidation of BN tubes by H_2O_2 at high temperature and high pressure.[10c] In turn, the relative intensity of the O1s core level spectrum was significantly increased after 100 h reaction time. This peak enhancement can be attributed to oxidation of boron atoms by hydroxyl radicals formed during the photo-Fenton reaction.[5a,15a,d,18] In addition, the XPS analyses of the supernatants of hBN samples, treated with P.F. reaction for 40 and 100 h, also supported the degradation of hBN sheets (Figure S12,S13 and Tables S2,S3). Indeed, XPS shows the presence of soluble boron species in both supernatants. Overall, the XPS analyses confirmed the strong oxidation of BN sheets during P.F. reaction most likely by breaking B–N bonds and forming new B–O bonds.

Finally, FT-IR spectroscopy was used to analyze the oxidation of hBN nanosheets by the P.F. reaction (Figure 5). The starting hBN nanosheets are mainly characterized by the B–N in-plane stretching and B-N-B bending vibrations at 1370 and 810 cm^{-1}, respectively.[18,19] However, after 40 h the

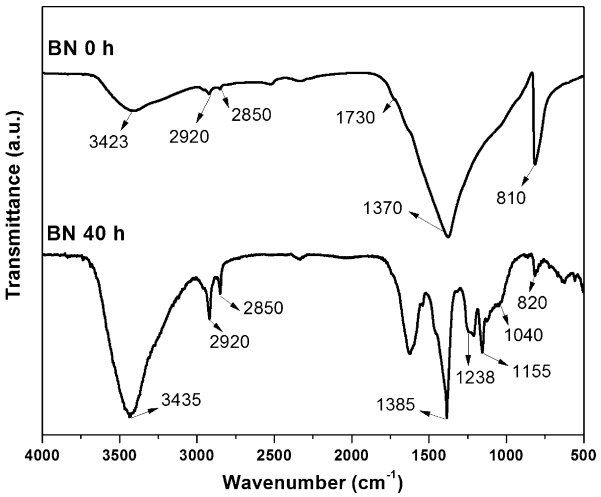

Figure 5. FT-IR spectra of hBN nanosheets treated under photo-Fenton reaction conditions for 0 h (top) and 40 h (bottom).

two fundamental vibrations displayed much lower intensities and were slightly shifted to higher frequencies. The significant changes in the fundamental vibrations is mainly attributed to the covalent modification of B–N bonds by hydroxyl radicals via disruption of the sp^2 network or by breaking B–N bonds, as reported for functionalized BN sheets and BN nanotubes.[18,19] A substantial degree of dislocation of the lattice is indeed possible because of the addition of OH groups to boron atoms.[18] In addition, new peaks can be observed after 40 h treatment; in particular the peak at 1155 cm^{-1} corresponding to B-O-H bending vibrations,[5a,20] and other prominent peaks at 1238 and 1040 cm^{-1} assigned to the in-plane bending vibrations of B–OH and symmetric B–O stretching, respectively.[18] The peaks between 700 to 500 cm^{-1} are related

to B-O-B bonds.[16] Thus, these additional features confirmed the oxidation of B–N to B–O and the presence of B–OH groups at the surface of the degrading material. The combined results of XPS and FT-IR confirmed the covalent functionalization of hBN by HO• generated during P.F. reaction.

The combination of the different analytical techniques applied in this work strongly supports the oxidative degradation of hBN nanosheets. Previous studies reported that the oxidation mechanism of hBN materials is different from graphene. The gradual substitution of N atoms by oxygen was expected during oxidation of BN, whereas the oxidation of graphene occurs mainly via epoxide bond formation.[21] Since the B–N bond is partially ionic, hydrolysis of BN occurs by addition of OH groups to the electron-deficient B atoms as demonstrated using ultra-sonication in water, which also results in cutting large BN planes into smaller sheets.[5a,22] The oxidation of B–N bonds was hypothesized to start at the defect sites, and then progress to the adjacent borazine units until reaching the edges and forming smaller and smaller fragments.[14,22] Hence, we believe that the degradation of our hBN nanosheets by reactive intermediates generated during the three oxidation treatments (HRP, MPO, and P.F.) can also proceed in the same way by breaking B–N bonds via B–O bond formation.

Raman and TEM results revealed that the degradation of hBN was rather limited by HRP treatment, while it was quite significant using MPO and nearly complete by the P.F. reaction. Therefore, the degree of hBN degradation/oxidation of BN sheets could be correlated to the redox potentials (E^o) of the reactive radicals generated and of the intermediates during the enzymatic catalysis of HRP, MPO and the UV action of the P.F. reaction. The redox potentials of HRP intermediates (compound I and II) are closed to 0.95 V, while MPO compound I and II have a potential of 1.16 and 1.34 V, respectively.[23] In addition, the much stronger oxidant HOCl is generated (1.48 V) during the catalytic process of MPO. As a consequence, a significant amount of hBN fragments were observed during MPO treatment compared to HRP. Similar results are reported for the degradation of CNTs or GO by the same enzymes.[9a,b] However, hydroxyl radicals generated in the P.F. reaction are the most powerful oxidants, with a redox potential of 2.31 V.[15a] Thus, a complete oxidation leading to degradation is possible by the P.F. reaction. This is plausible because a higher redox potential of BN sheets is predicted compared to graphitic materials (i.e. CNTs: 0.5 V), since hBN sheets have a much wider band gap than carbon nanotubes.[23] In general, compared to CNTs and GO, the degradation of hBN sheets is more challenging owing to the stronger oxidation resistance of BN over graphitic materials.[5d] For instance, graphene undergoes thermal oxidation at 450 °C, while BN monolayer are oxidized only at 850 °C.[5d] In previous studies, monolayer BN quantum dots were obtained by disintegrating bulk hBN via in situ generation of the strong oxidant KO_2.[16,24] Moreover, KO_2 was responsible for doping BN sheets with oxygen forming B–O bonds.[16] The hydroxyl radicals formed during the ultrasonication could be involved in scissoring BN sheets into smaller size.[22,25] Therefore, strong oxidants like KO_2 and HO• are needed to oxidize hBN. This is the reason why an extensive degradation of BN sheets was absent in the case of HRP unlike MPO and P.F. treatments.

The possible oxidation routes of hBN by the three types of oxidative treatments are hypothesized in Figure 1. In the case of HRP, the oxidation of the BN sheet is mainly limited to the edges (Figure 1, structure B) as confirmed by TEM images (Figure 3C). Highly porous sheets (Figure 1, structure C) were instead observed by MPO treatment for 35 h or P.F. reaction for 53 h (Figure 3E,H). Further oxidation by P.F. reaction up to 100 h resulted in a nearly complete degradation of the porous sheets into molecular or nanoscale BN fragments (Figure 3I), mainly consisting of B–O bonds (Figure 1, structure D). As explained above, the oxidation of hBN nanosheets could progress via substitution of N atoms by O, leading to form N defect sites ($BN_{3-x}O_x$ with $x = 1,2,3$), finally generating B_2O_3-like structures.[21a,26] In addition to the different types of oxidation treatments, the presence of aggregated or multilayered BN nanosheets also played a key role in the degradation as we observed in the Figure 3F (for MPO) and Figure S8 (for P.F.). Indeed, these aggregated/multilayered forms were not efficiently degraded compared to mono- or few-layer sheets. These kind of results were also observed for GO materials.[9b] Thus, layer thickness is also important during the biodegradation process.

In summary, we have reported for the first time the biodegradability of hBN nanosheets using two different types of peroxidases and the UV-assisted photo-Fenton reaction. Although hBN is quite resistant to HRP, significant degradation by human myeloperoxidase indicates that biodegradation of this material is possible in the organs that contain high levels of this enzyme (i.e. lungs).[9a,b] Future biodegradation studies of BN in activated immune cells like neutrophils and macrophages (where MPO is highly expressed) could give more insights about the biopersistance of BN materials in living species. In addition, the almost complete degradation by the photo-Fenton reaction suggests that an extensive oxidation of hBN nanosheets needs much more powerful oxidants, such as hydroxyl radicals. This behavior is highly useful to envisage strategies to decompose BN materials produced at industrial scales. In perspective, the synthesis of porous or functionalized BN sheets by controlling the photo-Fenton reaction duration might be of great interest to produce new polymer composites.[20a,27]

Acknowledgements

This work was supported by the Centre National de la Recherche Scientifique (CNRS), by the Agence Nationale de la Recherche (ANR) through the LabEx project Chemistry of Complex Systems (ANR-10-LABX-0026_CSC), and by the International Center for Frontier Research in Chemistry (icFRC). We gratefully acknowledge financial support from EU FP7-ICT-2013-FET-F GRAPHENE Flagship project (No. 604391). We wish to acknowledge Petra Hellwig and Frédéric Melin for giving access to Raman instrument, Cathy Royer and Valérie Demais for TEM analyses at the Plateforme Imagerie in Vitro at the Center of Neurochemistry (Strasbourg, France). We would like to thank Dris Ihiawakrim

for HRTEM and SAED measurements. We are also indebted to Fanny Bonachera for helping to prepare the BN structures and Isabella Anna Vacchi for XPS measurements.

Keywords: degradation · Fenton reaction · graphene-related materials · hexagonal boron nitride · peroxidases

How to cite: *Angew. Chem. Int. Ed.* **2016**, *55*, 5506–5511
Angew. Chem. **2016**, *128*, 5596–5601

[1] a) A. Geim, K. Novoselov, *Nat. Mater.* **2007**, *6*, 183–191; b) M. Chhowalla, H. S. Shin, G. Eda, L.-J. Li, K. P. Loh, H. Zhang, *Nat. Chem.* **2013**, *5*, 263–275; c) V. Nicolosi, M. Chhowalla, M. G. Kanatzidis, M. S. Strano, J. N. Coleman, *Science* **2013**, *340*, 1226419.

[2] a) H. Wang, X. Yang, W. Shao, S. Chen, J. Xie, X. Zhang, J. Wang, Y. Xie, *J. Am. Chem. Soc.* **2015**, *137*, 11376–11382; b) R. Kurapati, K. Kostarelos, M. Prato, A. Bianco, *Adv. Mater.* **2016**, DOI: 10.1002/adma.201506306.

[3] L. Cao, *MRS Bull.* **2015**, *40*, 592–599.

[4] D. Chimene, D. L. Alge, A. K. Gaharwar, *Adv. Mater.* **2015**, *27*, 7261–7284.

[5] a) D. Lee, B. Lee, K. H. Park, H. J. Ryu, S. Jeon, S. H. Hong, *Nano Lett.* **2015**, *15*, 1238–1244; b) P. Ma, J. Spencer, *J. Mater. Sci.* **2015**, *50*, 313–323; c) Z. Liu, Y. Gong, W. Zhou, L. Ma, J. Yu, J. C. Idrobo, J. Jung, A. H. MacDonald, R. Vajtai, J. Lou, P. M. Ajayan, *Nat. Commun.* **2013**, *4*, 1–8; d) L. H. Li, J. Cervenka, K. Watanabe, T. Taniguchi, Y. Chen, *ACS Nano* **2014**, *8*, 1457–1462; e) Z. Kuang, Y. Chen, Y. Lu, L. Liu, S. Hu, S. Wen, Y. Mao, L. Zhang, *Small* **2015**, *11*, 1655–1659; f) W. L. Song, P. Wang, L. Cao, A. Anderson, M. J. Meziani, A. J. Farr, Y. P. Sun, *Angew. Chem. Int. Ed.* **2012**, *51*, 6498–6501; *Angew. Chem.* **2012**, *124*, 6604–6607.

[6] Q. Weng, B. Wang, X. Wang, N. Hanagata, X. Li, D. Liu, X. Wang, X. Jiang, Y. Bando, D. Golberg, *ACS Nano* **2014**, *8*, 6123–6130.

[7] R. Arup Kumer, P. Byoungnam, L. Kang Seok, P. Sung Young, I. Insik, *Nanotechnology* **2014**, *25*, 445603.

[8] K. Bhattacharya, S. P. Mukherjee, A. Gallud, S. C. Burkert, S. Bistarelli, S. Bellucci, M. Bottini, A. Star, B. Fadeel, *Nanomed. Nanotechnol. Biol. Med.* **2016**, *12*, 333–351.

[9] a) V. Kagan, N. Konduru, W. Feng, B. Allen, J. Conroy, Y. Volkov, I. Vlasova, N. Belikova, N. Yanamala, A. Kapralov, Y. Tyurina, J. Shi, E. Kisin, A. Murray, J. Franks, D. Stolz, P. Gou, J. Klein-Seetharaman, B. Fadeel, A. Star, A. Shvedova, *Nat. Nanotechnol.* **2010**, *5*, 354–359; b) R. Kurapati, J. Russier, M. A. Squillaci, E. Treossi, C. Ménard-Moyon, A. E. Del Rio-Castillo, E. Vazquez, P. Samorì, V. Palermo, A. Bianco, *Small* **2015**, *11*, 3985–3994; c) G. P. Kotchey, B. L. Allen, H. Vedala, N. Yanamala, A. A. Kapralov, Y. Y. Tyurina, J. Klein-Seetharaman, V. E. Kagan, A. Star, *ACS Nano* **2011**, *5*, 2098–2108.

[10] a) Y. Zhao, X. Wu, J. Yang, X. C. Zeng, *Phys. Chem. Chem. Phys.* **2012**, *14*, 5545–5550; b) Y. Chen, J. Zou, S. J. Campbell, G. Le Caer, *Appl. Phys. Lett.* **2004**, *84*, 2430–2432; c) C. Y. Zhi, Y. Bando, T. Terao, C. C. Tang, H. Kuwahara, D. Golberg, *Chem. Asian J.* **2009**, *4*, 1536–1540.

[11] a) B. L. Allen, G. P. Kotchey, Y. Chen, N. V. K. Yanamala, J. Klein-Seetharaman, V. E. Kagan, A. Star, *J. Am. Chem. Soc.* **2009**, *131*, 17194–17205; b) A. R. Sureshbabu, R. Kurapati, J. Russier, C. Ménard-Moyon, I. Bartolini, M. Meneghetti, K. Kostarelos, A. Bianco, *Biomaterials* **2015**, *72*, 20–28.

[12] J. Coleman, M. Lotya, A. O'Neill, S. Bergin, P. King, U. Khan, K. Young, A. Gaucher, S. De, R. Smith, I. Shvets, S. Arora, G. Stanton, H.-Y. Kim, K. Lee, G. Kim, G. Duesberg, T. Hallam, J. Boland, J. Wang, J. Donegan, J. Grunlan, G. Moriarty, A. Shmeliov, R. Nicholls, J. Perkins, E. Grieveson, K. Theuwissen, D. McComb, P. Nellist, *Science* **2011**, *331*, 568–571.

[13] R. J. Smith, P. J. King, M. Lotya, C. Wirtz, U. Khan, S. De, A. O'Neill, G. S. Duesberg, J. C. Grunlan, G. Moriarty, J. Chen, J. Wang, A. I. Minett, V. Nicolosi, J. N. Coleman, *Adv. Mater.* **2011**, *23*, 3944–3948.

[14] B. L. Allen, P. D. Kichambare, P. Gou, I. I. Vlasova, A. A. Kapralov, N. Konduru, V. E. Kagan, A. Star, *Nano Lett.* **2008**, *8*, 3899–3903.

[15] a) X. Zhou, Y. Zhang, C. Wang, X. Wu, Y. Yang, B. Zheng, H. Wu, S. Guo, J. Zhang, *ACS Nano* **2012**, *6*, 6592–6599; b) Q. Liao, J. Sun, L. Gao, *Chem. Lett.* **2007**, *36*, 1446–1447; c) Y. Feng, K. Lu, L. Mao, X. Guo, S. Gao, E. J. Petersen, *Water Res.* **2015**, *84*, 49–57; d) H. Bai, W. Jiang, G. P. Kotchey, W. A. Saidi, B. J. Bythell, J. M. Jarvis, A. G. Marshall, R. A. S. Robinson, A. Star, *J. Phys. Chem. C* **2014**, *118*, 10519–10529.

[16] L. Lin, Y. Xu, S. Zhang, I. M. Ross, A. C. M. Ong, D. A. Allwood, *Small* **2014**, *10*, 60–65.

[17] G. P. Kotchey, S. A. Hasan, A. A. Kapralov, S. H. Ha, K. Kim, A. A. Shvedova, V. E. Kagan, A. Star, *Acc. Chem. Res.* **2012**, *45*, 1770–1781.

[18] T. Sainsbury, A. Satti, P. May, Z. Wang, I. McGovern, Y. K. Gun'ko, J. Coleman, *J. Am. Chem. Soc.* **2012**, *134*, 18758–18771.

[19] H. Shin, J. Guan, M. Z. Zgierski, K. S. Kim, C. T. Kingston, B. Simard, *ACS Nano* **2015**, *9*, 12573–12582.

[20] a) C. Gautam, C. S. Tiwary, S. Jose, G. Brunetto, S. Ozden, S. Vinod, P. Raghavan, S. Biradar, D. S. Galvao, P. M. Ajayan, *ACS Nano* **2015**, *9*, 12088–12095; b) O. M. Moon, B. C. Kang, S. B. Lee, J. H. Boo, *Thin Solid Films* **2004**, *464–465*, 164–169.

[21] a) K. A. Simonov, N. A. Vinogradov, M. L. Ng, A. S. Vinogradov, N. Mårtensson, A. B. Preobrajenski, *Surf. Sci.* **2012**, *606*, 564–570; b) N. A. Vinogradov, K. Schulte, M. L. Ng, A. Mikkelsen, E. Lundgren, N. Mårtensson, A. B. Preobrajenski, *J. Phys. Chem. C* **2011**, *115*, 9568–9577.

[22] Y. Lin, T. V. Williams, T.-B. Xu, W. Cao, H. E. Elsayed-Ali, J. W. Connell, *J. Phys. Chem. C* **2011**, *115*, 2679–2685.

[23] C. F. Chiu, B. A. Barth, G. P. Kotchey, Y. Zhao, K. A. Gogick, W. A. Saidi, S. Petoud, A. Star, *J. Am. Chem. Soc.* **2013**, *135*, 13356–13364.

[24] a) L. Lin, S. Zhang, *Chem. Commun.* **2012**, *48*, 10177–10179; b) M. Hayyan, F. S. Mjalli, M. A. Hashim, I. M. AlNashef, X. M. Tan, *J. Electroanal. Chem.* **2011**, *657*, 150–157.

[25] N. Masuda, A. Maruyama, T. Eguchi, T. Hirakawa, Y. Murakami, *J. Phys. Chem. B* **2015**, *119*, 12887–12893.

[26] M. Petravic, R. Peter, I. Kavre, L. H. Li, Y. Chen, L.-J. Fan, Y.-W. Yang, *Phys. Chem. Chem. Phys.* **2010**, *12*, 15349–15353.

[27] R. Jan, P. May, A. P. Bell, A. Habib, U. Khan, J. N. Coleman, *Nanoscale* **2014**, *6*, 4889–4895.

Received: February 3, 2016
Published online: March 24, 2016

